Nonreversible Transition from Hexagonal to Wurtzite Phase of BN under High Pressure: Optical Properties of the Wurtzite Phase

A. Segura,[†] R. Cuscó,[‡] T. Taniguchi,[¶] K. Watanabe,[¶] G. Cassabois,[§] B. Gil,[§] and L. Artús*,[‡]

† *Departamento de Física Aplicada-ICMUV, Malta-Consolider Team, Universitat de València, 46100 Burjassot, Spain.*

‡*Institut Jaume Almera (ICTJA-CSIC), Consejo Superior de Investigaciones Científicas, 08028 Barcelona, Spain.*

¶*National Institute for Materials Science,1-1 Namiki, Tsukuba, 305-0044, Japan.*

§*Laboratoire Charles Coulomb (L2C), UMR 5221 CNRS-Université de Montpellier, F-34095, Montpellier, France.*

Nonreversible Transition from the Hexagonal to Wurtzite Phase of Boron Nitride under High Pressure: Optical Properties of the Wurtzite Phase
A. Segura, R. Cuscó, T. Taniguchi, K. Watanabe, G. Cassabois, B. Gil, and L. Artús
The Journal of Physical Chemistry C (2019) 123 (33), pag. 20167-20173 DOI: 10.1021/acs.jpcc.9b06163

Abstract

We present an infrared reflectance and transmission study of a pressure-induced phase transition of boron nitride from the hexagonal layered structure to the wurtzitic phase. The transition is completed at about 13 GPa. The phase transition is nonreversible and the optical features of the metastable wurtzitic phase are retained after a pressure cycle from 20.5 GPa down to ambient pressure. This allows the infrared-active optical phonons and the dielectric properties of the cold-pressed wurtzitic boron nitride sample to be studied over the whole range of pressures. Experimental permittivity values of $\varepsilon_0 = 6.65 \pm 0.03$ and $\varepsilon_\infty = 4.50 \pm 0.05$ are determined from fits to the reflectance spectra at ambient pressure. Accurate values of the refractive index in the mid-infrared and visible-ultraviolet regions are evaluated from the interference patterns. Contrary to the h-BN case, the refractive index of w-BN decreases slightly with pressure, on account of the much lower compressibility of the close-packed structure. The pressure coefficients for the longitudinal optical and transverse optical modes are determined and an overall good agreement with *ab-initio* calculations is found.

Introduction

Boron nitride (BN) is a material with an enormous technological interest due to its unique electronic and thermal conductivity properties. Similarly to C, BN occurs in several polymorphs, namely cubic zinc-blende type (c-BN), layered hexagonal (h-BN), wurtzite-type (w-BN), rhombohedral (r-BN) and monoclinic (m-BN).[1,2]

The most common polymorphs are h-BN and c-BN. The two-dimensional h-BN has attracted a great deal of interest with the surge of research on two-dimensional crystals and van der Waals heterostructures as a promising dielectric material for graphene-based electronic devices.[3,4] The capability of stacking layers of graphene and BN with high precision has led to the observation of new intriguing phenomena such as fractal minigap structure (Hofstader butterfly)[5] and unconventional superconductivity of graphene superlattices.[6] Graphite–h-BN van der Waals structures have also been shown to exhibit enhanced photo-electrocatalytic activity.[7] The overpotential for oxygen reduction reaction, which severely limits fuel cell efficiency, was significantly reduced by spin coating BN nanotubes and BN nanosheets on Au electrodes.[8] Given the technological interest of BN, a great deal of effort is being currently devoted to understand the fundamental BN growth mechanisms and to develop scalable synthesis methods for producing high-quality, large area BN thin films via catalytic thermal chemical vapor deposition (CVD) processes on transition-metal foil substrates.[3,9,10]

h-BN is considered to be the most stable BN polymorph at ambient conditions. c-BN, which can be synthesized at high pressure/high temperature conditions, displays very high hardness and thermal conductivity next to diamond, and its superior thermal and chemical stability makes it the choice material for applications in cutting tools for ferrous metals. A nanocomposite containing a mixture of c-BN and w-BN was reported to reach the same hardness as diamond.[11] A bond-flipping phase transition was proposed to produce superior indentation strength in w-BN and in the isostructural lonsdaleite (hexagonal diamond) compared to diamond.[12]

The wide bandgap of BN and the capability of n- and p-type doping makes it a promising

material for electronic and deep-UV optical devices operating at high temperature and high powers. The development of BN-based high-temperature, high-power electronic devices is in its early stages because of the difficulty in obtaining electronic grade *c*-BN thin films.[13] The wurtzitic phase of BN, which is isostructural to other group-III nitrides with optoelectronic applications such as GaN, AlN, and InN, is metastable and therefore it is difficult to obtain with conventional growth methods.

So far, investigations on *w*-BN have mainly focused on its remarkable mechanical properties such as hardness and elastic stiffness.[14,15] Only UV reflectance measurements of compacted nanoscale *w*-BN powder have been reported in the literature,[16] which suggested a $w-$BN bandgap of 8.7 eV, in good agreement with local density approximation (LDA) calculations of a direct bandgap around 8.5 eV.[17] These results highlight the potential of *w*-BN as a dielectric for integration in BN-based technologies. Further investigation of the material properties, particularly of its optical properties in the IR and visible range, is essential to provide data for the characterization and improvement of the material quality that will enable the realization of the full potential of BN-based optoelectronic technology.

As a consequence of the difficulty in growing high-purity specimens of the metastable wurtzitic phase, the physical properties of *w*-BN have been scarcely studied. This is in stark contrast with the layered hexagonal phase, where the indirect bandgap,[18,19] the dielectric properties,[20] and the dependence of phonon dynamics on temperature[21] and boron isotopic composition[22–25] have been studied to a high level of detail.

In a previous work, we investigated the pressure dependence of the infrared(IR)-active modes by means of IR reflectivity and absorption experiments in a diamond anvil cell (DAC).[26] While the hexagonal phase of BN remained stable up to 10 GPa, the pressure dependence measurements revealed a substantial softening of the *out-of-plane* A_{2u}(TO) mode associated with a dynamical buckling of the flat honeycomb layers.[26] Such buckling distortions of the lamellar crystals induce a lattice instability that plays a central role in pressure-induced phase transitions.[27] By increasing the pressure above 10 GPa, a pressure induced phase transition to *w*-BN

takes place that completes at about 13 GPa, in agreement with previous studies of sp^3 bond formation in cold pressed h-BN.[27] Interestingly, the phase transition is not reversible and the w-BN structure is maintained after releasing the pressure at ambient conditions, which allows us to investigate the optical properties of BN in the wurtzitic phase. Whereas lattice dynamics of other group-III–nitrides that crystallize in the wurtzite structure have been studied in detail under high pressure,[28–30] we present here the first study of the optical properties of w-BN in the IR-visible spectral range. Phonon frequencies, dielectric constants and Grüneisen parameters of w-BN over a wide range of pressures up to 20.5 GPa are determined from IR reflectance and transmission measurements. The results obtained are compared to density functional theory calculations.

Experimental and Modeling Methods

The experiments were performed on high quality h-BN single crystals that were synthesized at 4.5 GPa and 1500°C using barium boron nitride as a solvent in a modified belt-type high-pressure and high-temperature apparatus.[31] Samples of thickness around 10 μm were cleaved from h-BN single crystalline platelets. The samples were subjected to high pressure in a membrane diamond anvil cell (DAC)[32] equipped with type-IIac diamond anvils. Methanol-ethanol-water (16:3:1) and KBr were used as pressure transmitting media (PTM) in the near-infrared(NIR)-visible and mid-infrared (MIR) range, respectively. While the first PTM is known to be hydrostatic up to 10 GPa and quasihydrostatic up to 20 GPa, KBr has been reported to produce non-hydrostatic tensions.[33] Pressure was determined using the ruby linear scale,[34,35] and the pressure distribution in the KBr charged DAC was checked by placing several ruby bills in the cell. Between 10 and 20 GPa the standard deviation of the pressure linearly increases from about 2% to 10% of the average pressure. The h-BN samples underwent a pressure-induced phase transition to the wurtzite phase[27] at pressures around 13 GPa. From the spectrometer resolution (0.006 nm), the absolute accuracy of the pressure determination is ~ 0.16 GPa.

High pressure measurements on the w-BN phase were carried out up to 20.5 GPa. During the downstroke, the metastable w-BN phase remained down to ambient pressure. Optical measurements were performed in the NIR, visible, and ultraviolet (UV) range using a home-made microscopic bench with deuterium and halogen lamps, reflecting objectives, and several multichannel spectrometers to cover the 15000–45000 cm^{-1} spectral range. Optical measurements in the MIR (500–3000 cm^{-1}) were performed by means of Fourier Transform Infrared Spectroscopy (FTIR) using an Interspectrum TEO-400 Michelson interferometer module coupled to a non-commercial all-reflecting microscope optical bench and a 22-μm HgCdTe detector.[36]

Density functional perturbation theory (DFPT) calculations were performed in the LDA using the ABINIT code.[37] Troulliers-Martins pseudopotentials in the Teter-Pade parametrization were employed. Integration over the Brillouin zone was carried out using a $9 \times 9 \times 6$ Monkhorst-Pack grid, with an energy cut-off of 70 Hartree. Structural relaxation yields lattice parameters of $a = 2.532$ Å and $c = 4.188$ Å, within 0.6% of reported experimental values.[38] The theoretical model also accurately reproduces the values of the compressibility reported in Ref. 38, with only slight overestimation of 0.07% at 10 GPa and 0.3% at 20 GPa.

Results and Discussion

The h-BN → w-BN Phase Transition

At high pressure, the layered h-BN undergoes a phase transformation to the hexagonal close-packed w-BN. The stacking similarities between h-BN and w-BN favor the conversion through the formation of new out-of-plane bonds.[27,39] As pressure increases, the weakly bound layers of h-BN get close together and the N atoms buckle down along the c axis and form sp^3 bonds with the B atoms located directly below and with the three neighboring B atoms in the layer. This is illustrated in Fig. 1. Near K-edge spectroscopy using inelastic x-ray scattering revealed that at 14 GPa sp^3 bonding forms simultaneously in both crystallographic directions without relative displacement of the layers.[27] Unlike the c-BN structure, the c-axis bond of the w-BN formed

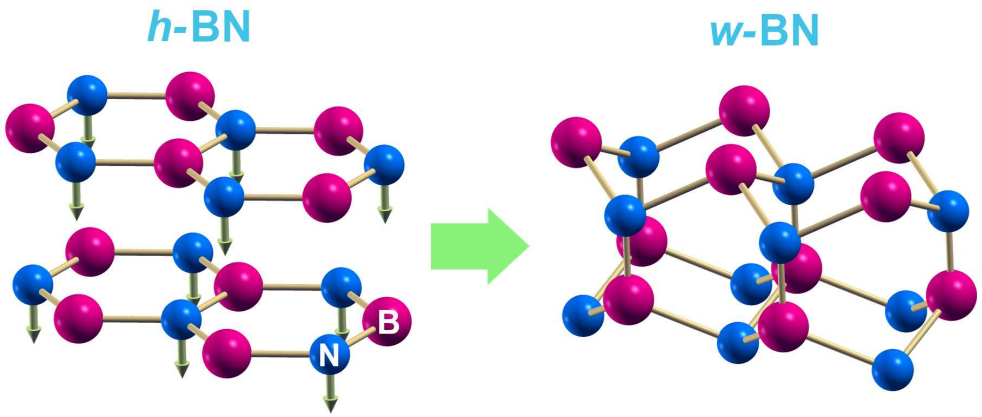

Figure 1: Phase transition pathway from hexagonal layered BN to the close-packed wurtzitic phase of BN under high pressure (~ 13 GPa) at room temperature. The arrows indicate the buckling of the nitrogen atoms under the constraint of no activation of relative lateral motion between the layers.

by compression displays some ionic character and is longer than the other bonds, which is a characteristic feature of the wurtzitic phase.[27]

In contrast, the h-BN to c-BN transformation would involve bond breaking and atom displacement to change the AA' stacking of h-BN to the ABC staggered stacking sequency of c-BN along the [111] direction. This suggests that such a phase transformation cannot be driven simply by compression.[39] Direct conversion from h-BN to c-BN has been disproved by high-resolution transmision electron microscopy studies.[40]

The reflectance spectrum of h-BN at normal incidence ($E \perp c$) displays a characteristic reststrahlen band in the 1360–1630 cm^{-1} range at ambient pressure, corresponding to the E_{1u} transverse-optical (TO) and longitudinal-optical (LO) modes of the hexagonal layered crystal.[26] The frequency of these modes were reported to increase with pressure coefficients of 3.4 and 4.0 cm^{-1} GPa^{-1} for pressures up to 10 GPa.[26] At higher pressures, a phase transition of the cold-pressed h-BN to w-BN begins to take place, which is evidenced by the quenching of the h-BN reststrahlen band and the emergence of a new reststrahlen band at lower frequencies, corresponding to the TO and LO modes of the w-BN crystal. This is illustrated in Fig. 2(b), where the infrared reflectance spectra of a cold-pressed h-BN sample are shown for the upstroke mea-

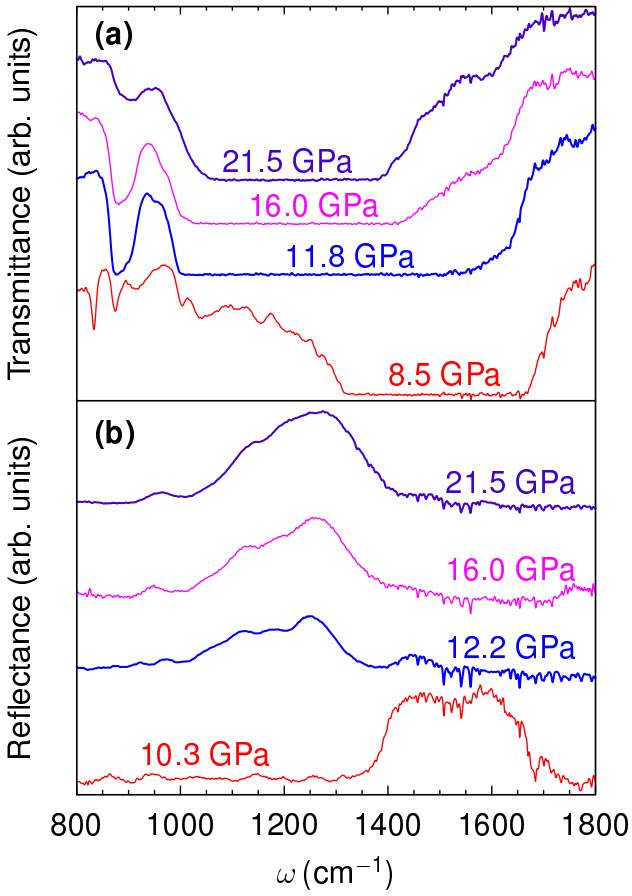

Figure 2: (a) IR transmission spectra of a BN sample recorded in the upstroke measurement at several pressures over the range where the h-BN → w-BN transition takes place. (b) Reflectance spectra of a different BN sample at several pressures over the pressure range where the phase transition occurs.

surement over the pressure range where the phase transition takes place. The changes in the transmission spectra displayed in Fig. 2(a) are consistent with the observed changes in the reflectance spectra. At 8.5 GPa, a region of nearly zero transmittance between 1320 and 1670 cm^{-1} is observed, which corresponds to the high reflectivity reststrahlen band of h-BN. At this pressure, the sample still retains the layered hexagonal structure. Indeed, the sharp absorption peak detected at ~ 835 cm^{-1} corresponds to the A_{2u}(LO) mode of h-BN.[26] As pressure is increased up to ~ 12 GPa, the nearly zero transmission region widens towards lower frequencies, indicating a progressive phase transformation of the sample to the w-BN structure. Concurrently, the A_{2u}(LO) absorption peak of h-BN vanishes and is barely visible in the 11.8 GPa transmission

spectrum. With a furher increase in pressure, the near zero transmission region narrows again but becomes centered at lower frequencies. At 21.5 GPa, it spans a spectral range from 1050 to 1380 cm^{-1}, which corresponds to the reststrahlen band of w-BN, thus indicating that the phase transition has been completed. The transmission spectra of the w-BN display a prominent absorption peak at around 900 cm^{-1}, which is particularly strong at pressures where the phase transition begins to take place (11.8 GPa spectrum). This absorption peak corresponds to a band of high density of lattice phonons of the wurtzitic structure (see Sec.), and therefore it is likely related to disorder activated modes in the highly defective w-BN phase.

The behavior of the reflectance spectra over the pressure range of the phase transition shown in Fig. 2(b) is consistent with the changes in the absorption observed in the sample discussed above. At 10.3 GPa the reststrahlen band spans a region between 1400 and 1660 cm^{-1}, in accord with previously published data on h-BN,[26] which indicates that the sample still retains the hexagonal phase. At higher pressures, this high reflectivity band vanishes and a new reststrahlen band emerges at lower frequencies. The latter spans a spectral region from about 1020 to 1350 cm^{-1} at 12.2 GPa, and shifts to higher frequencies with increasing pressure to stretch from about 1050 to 1380 cm^{-1} at 21.5 GPa.

The phase transition that we observe at $\sim$ 13 GPa is consistent with the quenching of the E_{2g} mode reported by Saha *et al.*[41] in Raman experiments at similar pressures. However, the h-BN $\rightarrow$ w-BN phase transition was not fully characterized in that work because none of the Raman active modes of w-BN was displayed: the A_1(LO) could not be measured because it lays in the region of large scattering by the Γ_{25} mode of diamond and the E_2 mode is out of the frequency range of the Raman spectra shown. From the limited experimental data shown in Ref. 41, the authors surmise a *reversible* phase transition from h-BN to w-BN. As we shall see below, our reflectance measurements unambiguously identify the w-BN phase formed at high pressure and, contrary to the interpretation made in Ref. 41, show that the phase transition is not reversible, with the metastable w-BN phase remaining down to ambient pressure.

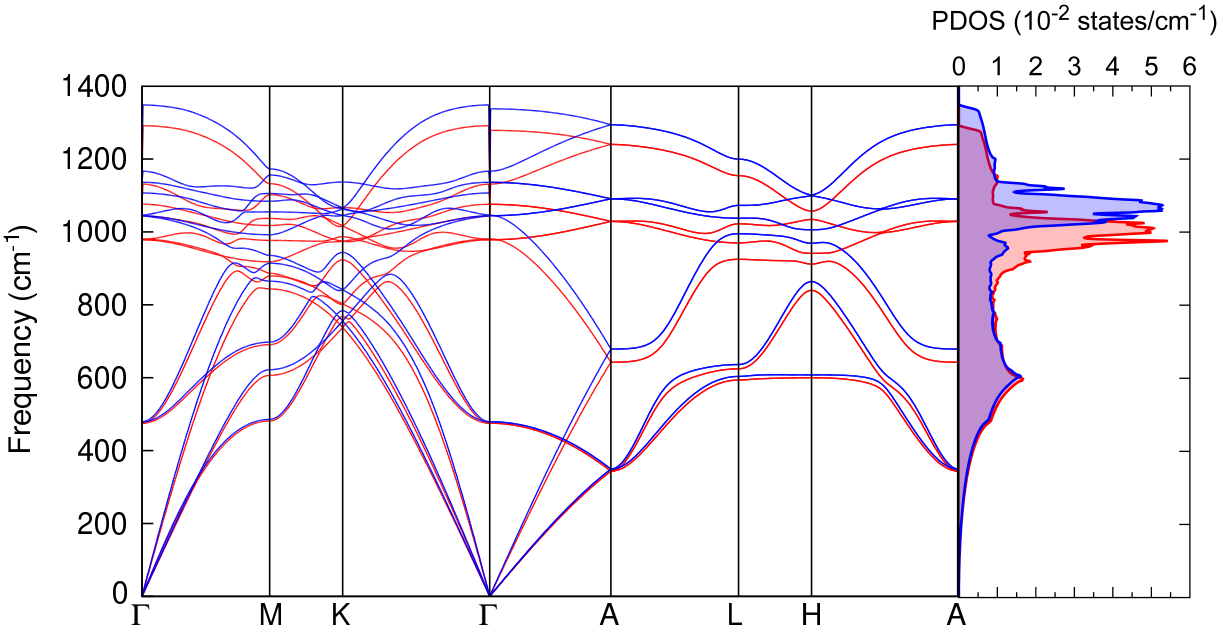

Figure 3: Phonon dispersion and phonon density of states of w-BN calculated using density functional perturbation theory at ambient pressure (red lines) and at 20 GPa (blue lines).

Phonon Dispersion of w-BN

Figure 3 displays the phonon dispersion and phonon density of states of w-BN calculated at ambient pressure (red lines) and at 20 GPa (blue lines). The optical-mode phonon frequencies exhibit a nearly linear increase with pressure. The values of phonon frequencies at ambient pressure are in good agreement with previous *ab-initio* calculations on w-BN..[42,43] We find a bulk modulus of B = 399 GPa, in good agreement with previous calculations,[42,43] but about 20% higher than the value recently estimated in nanoindentation experiments by Deura *et al.*[15] For convenience, the zone-center phonon frequencies calculated at ambient pressure together with pressure coefficients and Grüneisen parameters are listed in Table 1. All phonons exhibit similar pressure coefficients, except for the low-frequency E_2 mode, which is fairly insensitive to pressure, and the high-frequency silent mode (B_1), which has a somewhat smaller pressure coefficient. A distinct feature can be seen at ~ 956 cm^{-1} in the phonon density of states at high pressure. This feature, which has a pressure coefficient of ~ 2 cm^{-1} GPa^{-1}, emerges at

high pressures due to the flat silent mode bands close to the M and H points becoming well-separated from neighboring TO bands.

Irreversibility of the *h*-BN → *w*-BN Phase Transition

Figure 4 displays the reflectance spectrum at normal incidence of the *w*-BN sample at 20.5 GPa, when the wurtzitic phase has been fully stabilized, and the reflectance spectrum at ambient pressure recorded at the end of the downstroke cycle outside the DAC. For comparison, the distinct spectrum of the *h*-BN, which displays the reststrahlen band at higher frequencies, is also shown. These results unambiguously show that the *h*-BN → *w*-BN pressure-induced phase transition is not reversible upon pressure release after the stabilization of the wurtzitic phase at high pressure. This is contrary to the prior suggestion that the pressure-induced *h*-BN → *w*-BN phase transition could be reversed by releasing the pressure.[41] *w*-BN is predicted to be a metastable phase at ambient conditions, with a zero-temperature energy that is sizeably larger than those of *c*-BN and *h*-BN.[2] However, the kinetic constraint at ambient temperature restricting the relative rotation and displacement of the *h*-BN layers was shown to favor the formation of *w*-BN under cold compression.[27] Kinetic constraints as well as the presence of stabilizing defects in the pressure-induced wurtzitic phase may contribute to promote the prevalence of the *w*-BN phase in the transited sample at ambient pressure.

Table 1: Values of the Phonon Frequency ω (in cm^{-1}) at Ambient Pressure, Pressure Coefficient $d\omega/dP$ (in cm^{-1} GPa^{-1}) and Grüneisen Parameter γ for the Zone-Center Optical Phonons of *w*-BN Derived from DFPT Calculations.

	E_2	E_2	B_1	A_1(TO)	E_1(TO)	B_1	A_1(LO)	E_1(LO)
ω	475.1	978.6	981.3	1043.4	1075.9	1131.3	1278.9	1291.5
$d\omega/dP$	0.21	3.52	3.53	3.41	3.21	1.86	3.16	3.02
γ	0.18	1.43	1.44	1.30	1.19	0.66	0.99	0.93

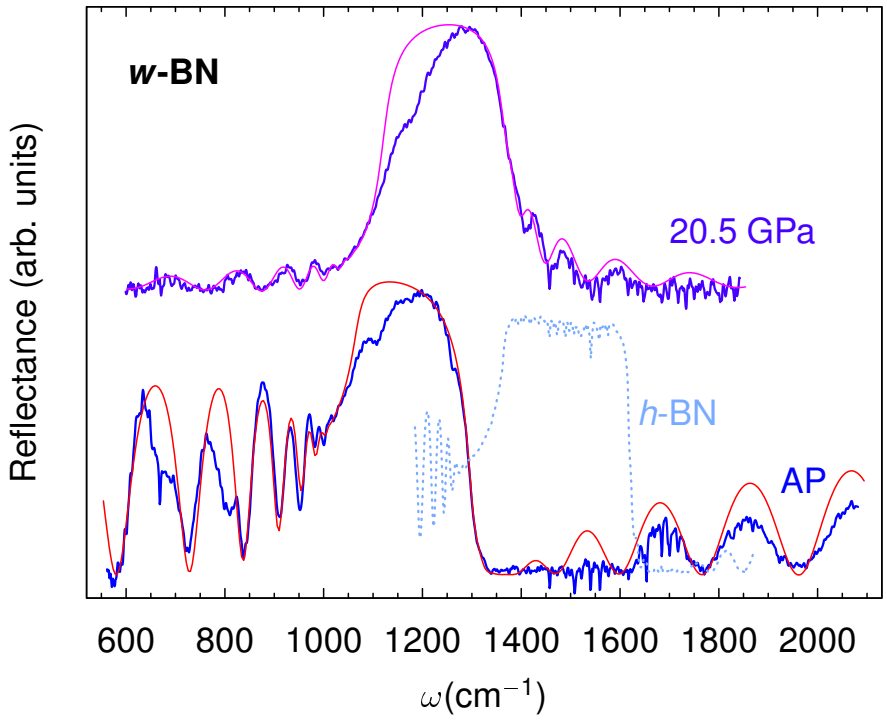

Figure 4: Reflectance spectra at normal incidence ($E \perp c$) of w-BN at 20.5 GPa and of the cold-pressed w-BN sample at ambient pressure outside the diamond anvil cell. The reflectance calculated using the dielectric model is displayed as magenta and red lines. For comparison, the reflectance spectra of the original h-BN crystal is also shown as a dotted line.

Dielectric Properties: Refractive Index Dispersion of *w*-BN

Information about the dielectric properties of w-BN is obtained by fitting a reflectivity model that takes into account the contribution of the polar modes to the dielectric function

$$\varepsilon(\omega) = \varepsilon_\infty + (\varepsilon_0 - \varepsilon_\infty)\frac{\omega_{\mathrm{TO}}^2}{\omega_{\mathrm{TO}}^2 - \omega^2 - i\Gamma\omega}. \tag{1}$$

Here ε_0 is the static dielectric constant, ε_∞ is the electronic dielectric constant, and ω_{TO} and Γ are the frequency and damping parameter of the TO mode. From Eq. (1), the real and imaginary parts of the refractive index are determined, and then the reflectance is calculated and fitted to the experimental data. At ambient pressure, the TO and LO frequencies fitted to the spectra are 1068 and 1298 cm^{-1}, respectively, within less than 1% deviation from the E_1 frequencies predicted by DFPT calculations (see Table 1). The calculated *in-plane* (perpendicular

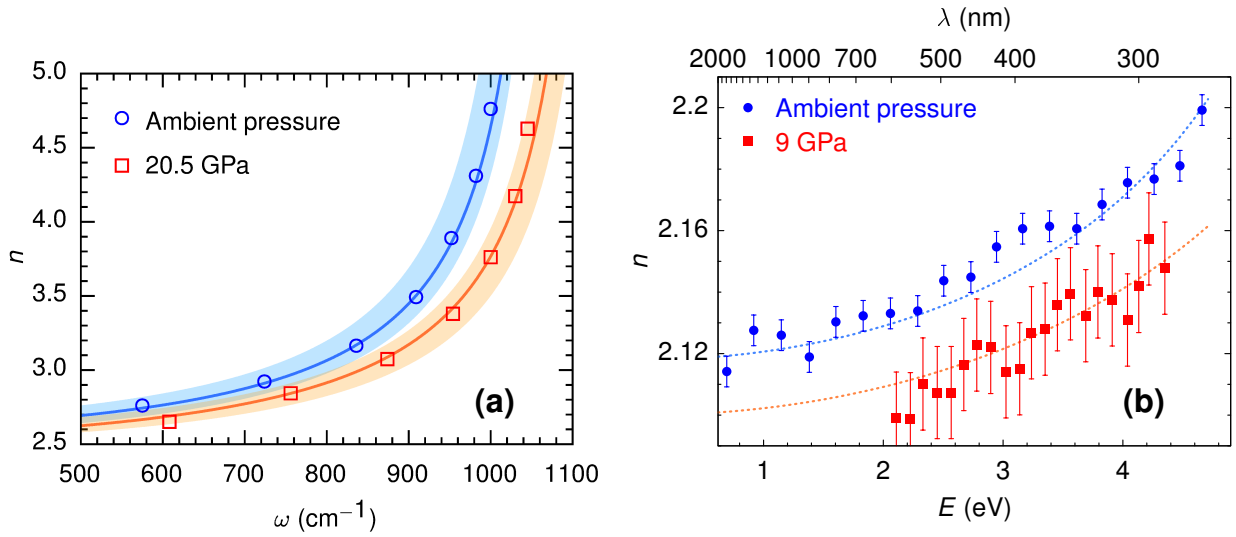

Figure 5: (a) Dispersion of the refractive index of w-BN close to the TO resonance at ambient pressure and at 20.5 GPa. The values obtained from the interference pattern are plotted with symbols and the values derived from the fit to the IR reflectance spectra are displayed as solid lines. The error bars at 20.5 GPa correspond to the size of the symbols, whereas at ambient pressure the error bars are about four times smaller. The shaded areas correspond to the region between the *out-of-plane* and *in-plane* refractive indices as given by the DFPT calculations. (b) Dispersion of the refractive index in the near-IR to UV spectral region at ambien pressure and at 9 GPa. The dotted lines are guides to the eye.

to the c axis) static and electronic dielectric constants, $\varepsilon_0^{\perp} = 6.44$ and $\varepsilon_\infty^{\perp} = 4.47$, are also in good agreement with the values fitted to the reflectance spectrum as explained below, which yield values of 6.65 ± 0.03 and 4.50 ± 0.05, respectively. A relatively large damping parameter of $\Gamma = 24$ cm^{-1} was used in the fit. This is in contrast with the low damping of ~ 4 cm^{-1} found for the E_{1u} mode in h-BN.[26] The higher damping and the loss of uniformity in the reflectivity across the reststrahlen band observed in the w-BN sample are likely related to the large presence of defects in the pressure-stabilized metastable phase.

The dispersion of the refractive index below the TO frequency derived from the fits to the IR reflectance is plotted in Fig. 5(a) as solid lines for ambient pressure (blue) and at 20.5 GPa (red). The refractive index can be evaluated also from the reflectivity oscillations arising from the multiple reflections in the lamellar sample, which yield minima at $2n(\omega)d = K\lambda$, where the interference order K and the sample thickness d can be self-consistently determined. The thickness

of the w-BN sample was determined to be 9.26μm at 20 GPa and 9.41μm at ambient pressure. The sample thickness increase upon releasing pressure is in excellent agreement with the calculated pressure dependence of the lattice parameters and with experimental determinations of the equation of state of w-BN.[38] The accurate values of the refractive index obtained from the interference minima are displayed as symbols in Fig. 5(a). They are in excellent agreement with the values derived from the fit to the reflectance spectra, thus confirming the consistency of the analysis of the IR data.

The experimental values of the refractive index lie between the *out-of-plane* and *in-plane* refractive index values predicted by the DFPT calculations, which are determined, respectively, by the A_1 and E_1 polar phonons. It cannot be ruled out that the transited sample contains misoriented crystallites and therefore the reflectance experiments at normal incidence with $E \perp c$ may probe an effective dielectric constant with some *out-of-plane* contribution. Figure 5(b) shows the refractive index in the near-IR to UV spectral region at ambient pressure and at 9 GPa derived from the interference pattern. In the reflectance spectra, the interference minima are used since they are better defined and correspond to integer orders. Conversely, in the transmission spectra in the visible-UV region, the interference maxima are better defined and they are used to determine the refractive index. Data at 9 GPa include both the values calculated at the interference maxima and minima to enhance the statistical significance. The refractive index of w-BN displays a slight positive dispersion in this energy range, much lower than that of its h-BN counterpart.[20] According to electronic bandstructure calculations of w-BN found in the literature,[17,44,45] the direct bandgap of the wurtzitic phase is much larger than for the hexagonal phase. Consequently, the variation of the refractive index in the UV region is much smaller in w-BN than in h-BN.[20] However, the magnitude of the optical gaps in the theoretically calculated electronic bandstructure of w-BN would suggest a stronger energy dependence. While the LDA may significantly underestimate the optical gaps, it cannot be ruled out that the presence of misoriented domains in the transited sample may introduce a sizable contribution of the extraordinary refractive index.

Contrary to the hexagonal phase, the refractive index in the wurtzitic phase shows a slight decrease with pressure. The different dielectric behavior of these two phases is exemplified by the markedly different values of the dielectric constants and their opposite pressure dependence. Whereas ε_∞ increases with pressure in h-BN with a pressure coefficient of 4.7×10^{-2} GPa^{-1}, the pressure coefficient is much smaller and negative in w-BN ($d\varepsilon/dP = -(8 \pm 1) \times 10^{-3}$ GPa^{-1}). This is consistent with the DFPT calculations, which yield a pressure coefficient of -2×10^{-3} GPa. The large positive pressure coefficient of the refractive index of h-BN stems from the large compressibility of the layered structure ($B \sim 26$ GPa), which leads to a significant increase of the density of polarizable units. The covalently-bonded, close-packed w-BN polymorph has a much lower compressibility ($B \sim 399$ GPa), and the increase in density of polarizable units is overcompensated by the strong blueshift of the optical gaps.[46]

Vibrational Properties of *w*-BN: Pressure Coefficients of IR-Active Phonons

Figure 6 shows the pressure dependence of the phonon frequencies obtained from the fits to the IR reflectance spectra taken on the downstroke cycle from 20.5 GPa to ambient pressure. The IR reflectance spectra at both ends of the pressure cycle are displayed in Fig. 4, illustrating the downshift of the reststrahlen band with decreasing pressure. The TO frequencies derived from the fits to the IR reflectance spectra are somewhat lower than the E_1(TO) values predicted by the DFTP calculations, and lie between the A_1(TO) and E_1(TO) frequencies (see Table 1). While this discrepancy might be due to uncertainties in the analysis of the reflectance spectra and to the typical margin of error in the calculated values, the mixing of A_1 and E_1 modes in disoriented crystallytes present in the transited sample could also contribute to the effective lower TO frequency extracted from the reflectance spectra. The data show a regular trend of phonon frequency increase with pressure that follows closely the theoretical predictions, suggesting that nonhydrostatic behavior of the PTM at the highest pressures does not substantially alter the measured phonon frequencies. The pressure coefficient $d\omega_{TO}/dP = 2.8 \pm 0.1$ cm^{-1} GPa^{-1} obtained from the IR measurements agrees very well with the pressure dependence of

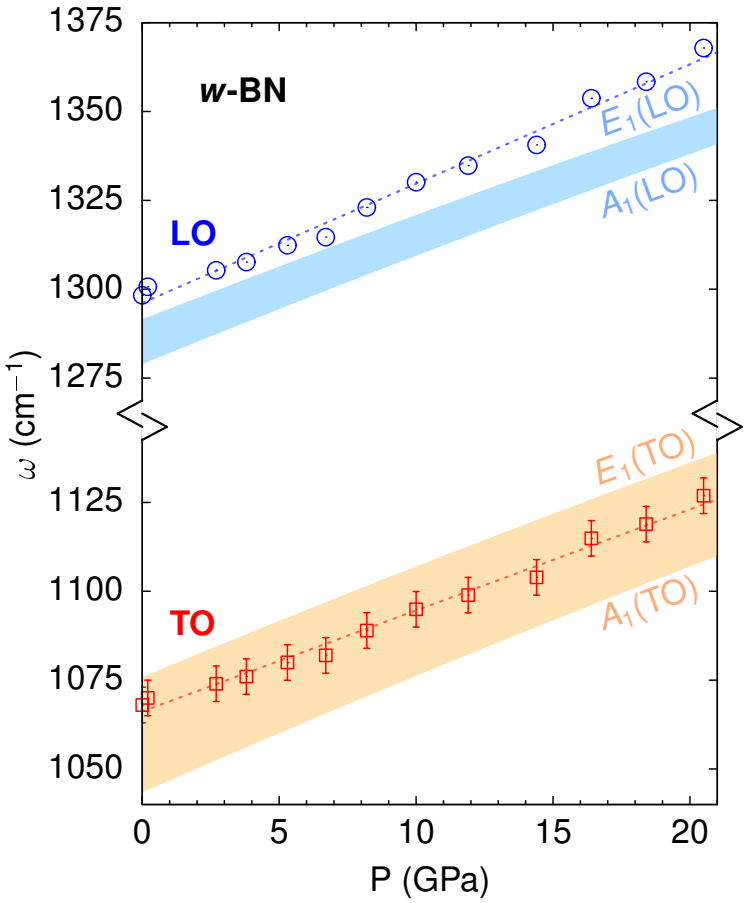

Figure 6: Pressure dependence of the TO (squares) and LO phonons (circles) of w-BN derived from the IR reflectance measurements. The error bars for the LO frequencies correspond to the size of the symbols. The dotted lines are linear fits to the data. The shaded areas indicate the region between the A_1 and E_1 frequencies of the TO (orange) and LO (cyan) modes obtained from *ab-initio* calculations.

the TO modes predicted by DFPT. A pressure coefficient $d\omega_{\mathrm{LO}}/dP = 3.4 \pm 0.1$ cm^{-1} GPa^{-1} is found for the LO mode frequencies, which lie slightly above the A_1(LO)–E_1(LO) region. The underestimation of the LO-TO splitting is commonplace in LDA calculations and it has been related to the well-known LDA bandgap problem.[47]

These pressure coefficients are somewhat lower than those reported for the *in-plane* optical modes of h-BN (3.4 and 4.0 cm^{-1} GPa^{-1} for E_{1u} TO and LO modes, respectively),[26] owing to the more close-packed structure and lower compressibility of the wurtzite phase. The pressure coefficients found for w-BN are also lower than those reported in other group-III–nitrides,[29] on

account of the lower compressibility of the w-BN crystal.

Conclusions

The metastable close-packed wurtzitic phase of BN is stabilized under high pressure at room temperature. After a pressure cycle up to 21 GPa, the wurtzitic phase of BN remains stable at ambient conditions. The phase transition from h-BN to w-BN that takes place at around 13 GPa has been characterized by IR reflectance and transmittance measurements. Our results show unambiguously that the h-BN $\rightarrow$ w-BN transition is not reversible. Since the wurtzitic phase is maintained down to ambient pressure, we have been able to investigate the infrared-active optical phonons and the dielectric properties of w-BN over the whole pressure range from ambient pressure to 20.5 GPa.

At ambient pressure, the static and electronic dielectric constants are determined as $\varepsilon_0 = 6.65 \pm 0.03$ and $\varepsilon_\infty = 4.50 \pm 0.05$ from fits to the reflectance spectra, in good agreement with the *out-of-plane* dielectric constants calculated by DFPT. To our knowledge, this is the first study to examine and systematically characterize the optical and dielectric properties of w-BN.

The refractive index dispersion has been determined to a high accuracy in the MIR and in the NIR-UV spectral regions using the interference pattern in the thin platelets. In the NIR-UV range, the refractive index of w-BN displays a slight positive dispersion that is much lower than in its h-BN counterpart. In contrast with the substantial increase in the dielectric constants with pressure reported in h-BN, the dielectric constants decrease slightly with increasing pressure in w-BN. This different dielectric behavior is attributed to the vastly different compressibility of both structures.

The pressure coefficients found for the IR-active optical phonons of w-BN are similar but somewhat lower than those of the *in-plane* polarized phonons of h-BN. The IR results are in overall good agreement with theoretical predictions based on DFPT calculations.

Acknowledgements

This work has been supported by the Spanish MINECO/FEDER under Contracts No.MAT2015-71035-R and No. MAT2016-75586-C4-1-P. T. T. acknowledges support from the Elemental Strategy Initiative conducted by the MEXT, Japan and JSPS KAKENHI Grant Number JP15K21722. B. G. acknowledges support from the Government of the Russian Federation, contract #14.W03.31.0011 at Ioffe Institute.

References

(1) Izyumskaya, N.; Demchenko, D. O.; Das, S.; Ozgur, U.; Avrutin, V.; Morkoc, H. Recent Development of Boron Nitride towards Electronic Applications. *Adv. Elecron. Mater.* **2017**, *3*, 1600485.

(2) Cazorla, C.; Gould, T. Polymorphism of Bulk Boron Nitride. *Sci. Adv.* **2019**, *5*, eaau5832.

(3) Bresnehan, M. S.; Hollander, M. J.; Wetherington, M.; LaBella, M.; Trumbull, K. A.; Cavalero, R.; Snyder, D. W.; Robinson, J. A. Integration of Hexagonal Boron Nitride with Quasi-freestanding Epitaxial Graphene: Toward Wafer-Scale, High-Performance Devices. *ACS Nano* **2012**, *6*, 5234–5241.

(4) Geim, A. K.; Grigorieva, I. V. Van der Waals Heterostructures. *Nature* **2013**, *499*, 419–425.

(5) Ponomarenko, L. A.; Gorbachev, R. V.; Yu, G. L.; Elias, D. C.; Jalil, R.; Patel, A. A.; Mishchenko, A.; Mayorov, A. S.; Woods, C. R.; Wallbank, J. R. et al. Cloning of Dirac fermions in graphene superlattices. *Nature* **2013**, *497*, 594–597.

(6) Cao, Y.; Fatemi, V.; Fang, S.; Watanabe, K.; Taniguchi, T.; Kaxiras, E.; Jarillo-Herrero, P. Unconventional superconductivity in magic-angle graphene superlattices. *Nature* **2018**, *556*, 43–50.

(7) Bawari, S.; Pal, S.; Pal, S.; Mondal, J.; Narayanan, T. N. Enhanced Photo-Electrocatalytic Hydrogen Generation in Graphene/hBN van der Waals Structures. *J. Phys. Chem. C* **2019**, *123*, 17249–17254

(8) Elumalai, G.; Noguchi, H.; Uosaki, K. Electrocatalytic activity of various types of h-BN for the oxygen reduction reaction. *Phys. Chem. Chem. Phys.* **2014**, *16*, 13755–13761.

(9) Müller, F.; Stöwe, K.; Sachdev, H. Symmetry versus Commensurability: Epitaxial Growth of Hexagonal Boron Nitride on Pt(111) From B-Trichloroborazine (ClBNH)3. *Chem. Mater.* **2005**, *17*, 3464–3467.

(10) Sutter, P.; Lahiri, J.; Albrecht, P.; Sutter, E. Chemical Vapor Deposition and Etching of High-Quality Monolayer Hexagonal Boron Nitride Films. *ACS Nano* **2011**, *5*, 7303–7309.

(11) Dubrovinskaia, N.; Solozhenko, V. L.; Miyajima, N.; Dmitriev, V.; Kurakevych, O. O.; Dubrovinsky, L. Superhard Nanocomposite of Dense Polymorphs of Boron Nitride: Non-Carbon Material has Reached Diamond Hardness. *Appl. Phys. Lett.* **2007**, *90*, 101912.

(12) Pan, Z.; Sun, H.; Zhang, Y.; Chen, C. Harder than Diamond: Superior Indentation Strength of Wurtzite BN and Lonsdaleite. *Phys. Rev. Lett.* **2009**, *102*, 055503.

(13) Zhang, X.; Boyen, H.; Deyneka, N.; Ziemann, P.; Banhart, F.; Schreck, M. Epitaxy of Cubic Boron Nitride on (001)-Oriented Diamond. *Nature Mater.* **2003**, *2*, 312–315.

(14) Nagakubo, A.; Ogi, H.; Sumiya, H.; Kusakabe, K.; Hirao, M. Elastic Constants of Cubic and Wurtzite Boron Nitrides. *Appl. Phys. Lett.* **2013**, *102*, 241909.

(15) Deura, M.; Kutsukake, K.; Ohno, Y.; Yonenaga, I.; Taniguchi, T. Nanoindentation Measurements of a Highly Oriented Wurtzite-Type Boron Nitride Bulk Crystal. *Jpn. J. Appl. Phys.* **2017**, *56*, 030301.

(16) Yixi, S.; Xin, J.; Kun, W.; Chaoshu, S.; Zhengfu, H.; Junyan, S.; Jie, D.; Sheng, Z.; Yuanbin, C.

Vacuum-ultraviolet reflectance spectra and optical properties of nanoscale wurtzite boron nitride. *Phys. Rev. B* **1994**, *50*, 18637–18639.

(17) Christensen, N. E.; Gorczyca, I. Optical and Structural Properties of III-V Nitrides under Pressure. *Phys. Rev. B* **1994**, *50*, 4397–4415.

(18) Cassabois, G.; Valvin, P.; Gil, B. Hexagonal Boron Nitride is an Indirect Bandgap Semiconductor. *Nat. Photonics* **2016**, *10*, 262–266.

(19) Vuong, T. Q. P.; Cassabois, G.; Valvin, P.; Jacques, V.; Cuscó, R.; Artús, L.; Gil, B. Overtones of Interlayer Shear Modes in the Phonon-Assisted Emission Spectrum of Hexagonal Boron Nitride. *Phys. Rev. B* **2017**, *95*, 045207.

(20) Segura, A.; Artús, L.; Cuscó, R.; Taniguchi, T.; Cassabois, G.; Gil, B. Natural Optical Anisotropy of h-BN: Highest Giant Birefringence in a Bulk Crystal through the Mid-Infrared to Ultraviolet Range. *Phys. Rev. Mater.* **2018**, *2*, 024001.

(21) Cuscó, R.; Gil, B.; Cassabois, G.; Artús, L. Temperature Dependence of Raman-Active Phonons and Anharmonic Interactions in Layered Hexagonal BN. *Phys. Rev. B* **2016**, *94*, 155435.

(22) Vuong, T. Q. P.; Liu, S.; van de Lee, A.; Cuscó, R.; Artús, L.; Michel, T.; Valvin, P.; Edgar, J. H.; Cassabois, G.; Gil, B. Isotope Engineering of van der Waals Interactions in Hexagonal Boron Nitride. *Nat. Mater.* **2018**, *17*, 152–158.

(23) Cuscó, R.; Artús, L.; Edgar, J. E.; Liu, S.; Cassabois, G.; Gil, B. Isotopic effects on phonon anharmonicity in layered van der Waals crystals: A study of isotopically pure hexagonal boron nitride. *Phys. Rev. B* **2018**, *97*, 155435.

(24) Cuscó, R.; Edgar, J. H.; Liu, S.; Cassabois, G.; Gil, B.; Artús, L. Influence of Isotopic Substitution on the Anharmonicity of the Interlayer Shear Mode of h -BN. *Phys. Rev. B* **2019**, *99*, 085428.

(25) Cuscó, R.; Edgar, J.; Liu, S.; Cassabois, G.; Gil, B.; Artús, L. Effects of Isotopic Substitution on the Phonons of van der Waals Crystals: the Case of Hexagonal Boron Nitride. *J. Phys. D: Appl. Phys.* **2019**, *52*, 303001.

(26) Segura, A.; Cuscó, R.; Taniguchi, T.; Watanabe, K.; Cassabois, G.; Gil, B.; Artús, L. High-Pressure Softening of the Out-of-Plane A2u(Transverse-Optic) Mode of Hexagonal Boron Nitride Induced by Dynamical Buckling. *J. Phys. Chem. C* **2019**, *123*, 17491–17497

(27) Meng, Y.; Mao, H.-k.; Eng, P. J.; Trainor, T. P.; Newville, M.; Hu, M. Y.; Kao, C.; Shu, J.; Hausermann, D.; Hemley, R. J. The Formation of sp^3 Bonding in Compressed BN. *Nat. Mater.* **2004**, *3*, 111–114.

(28) Xia, H.; Xia, Q.; Ruoff, A. L. High-pressure structure of gallium nitride: Wurtzite-to-rocksalt phase transition. *Phys. Rev. B* **1993**, *47*, 12925–12928.

(29) Manjón, F. J.; Errandonea, D.; Romero, A. H.; Garro, N.; Serrano, J.; Kuball, M. Lattice dynamics of wurtzite and rocksalt AlN under high pressure: Effect of compression on the crystal anisotropy of wurtzite-type semiconductors. *Phys. Rev. B* **2008**, *77*, 205204.

(30) Ibáñez, J.; Segura, A.; García-Domene, B.; Oliva, R.; Manjón, F. J.; Yamaguchi, T.; Nanishi, Y.; Artús, L. High-pressure optical absorption in InN: Electron density dependence in the wurtzite phase and reevaluation of the indirect band gap of rocksalt InN. *Phys. Rev. B* **2012**, *86*, 035210.

(31) Taniguchi, T.; Watanabe, K. Synthesis of High-Purity Boron Nitride Single Crystals under High Pressure by Using Ba-BN Solvent. *J. Cryst. Growth* **2007**, *303*, 525–529.

(32) Le Toullec, R.; Pinceaux, J.; Loubeyre, P. The Membrane Diamond Anvil Cell: A New Device for Generating Continuous Pressure and Temperature Variations. *High Pressure Res.* **1988**, *1*, 77–90.

(33) Zhao, J.; Ross, N. L. Non-Hydrostatic Behavior of KBr as a Pressure Medium in Diamond Anvil Cells up to 5.63 GPa. *J. Phys.: Condens. Matter* **2015**, *27*, 185402.

(34) Mao, H. K.; Xu, J.; Bell, P. M. Calibration of the Ruby Pressure Gauge to 800 kbar under Quasi-Hydrostatic Conditions. *J. Geophys. Res.* **1986**, *91*, 4673–4676.

(35) Chervin, J. C.; Canny, B.; Mancinelli, M. Ruby-Spheres as Pressure Gauge for Optically Transparent High Pressure Cells. *High Pressure Res.* **2001**, *21*, 305–314.

(36) Panchal, V.; Segura, A.; Pellicer-Porres, J. Low-Cost Set-Up for Fourier-Transform Infrared Spectroscopy in Diamond Anvil Cell from 4000 to 400 cm^{-1}. *High Pressure Res.* **2011**, *31*, 445–453.

(37) ABINIT is a common project of the Université Catholique de Louvain, Corning Incorporated, and other contributors (http://www.abinit.org). X. Gonze,; Beuken, J.-M.; Caracas, R.; Detraux, F.; Fuchs, M.; Rignanese, G.-M.; Sindic, L.; Verstraete, M.; Zerah, G.; Jollet, F. et al. First-principles computation of material properties: the ABINIT software project. *Comput. Mater. Sci.* **2002**, *25*, 478–492.

(38) Solozhenko, V. L.; Häusermann, D.; M., M.; Kunz, M. Equation of State of Wurtzitic Boron Nitride to 66 GPa. *Appl. Phys. Lett.* **1998**, *72*, 1691–1693.

(39) Tararan, A.; di Sabatino, S.; Gatti, M.; Taniguchi, T.; Watanabe, K.; Reining, L.; Tizei, L. H. G.; Kociak, M.; Zobelli, A. Optical Gap and Optically Active Intragap Defects in Cubic BN. *Phys. Rev. B* **2018**, *98*, 094106.

(40) Nistor, L. C.; Tendeloo, G. V.; Dinca, G. Crystallographic Aspects Related to the High Pressure–High Temperature Phase Transformation of Boron Nitride. *Philos. Mag.* **2005**, *85*, 1145–1158.

(41) Saha, S.; Muthu, D.; Golberg, D.; Tang, C.; Zhi, C.; Bando, Y.; Sood, A. Comparative High

Pressure Raman Study of Boron Nitride Nanotubes and Hexagonal Boron Nitride. *Chem. Phys. Lett.* **2006**, *421*, 86–90.

(42) Ohba, N.; Miwa, K.; Nagasako, N.; Fukumoto, A. First-Principles Study on Structural, Dielectric, and Dynamical Properties for Three BN Polytypes. *Phys. Rev. B* **2001**, *63*, 115207.

(43) Karch, K.; Bechstedt, F. Ab initio Lattice Dynamics of BN and AlN: Covalent versus Ionic Forces. *Phys. Rev. B* **1997**, *56*, 7404–7415.

(44) Park, K. T.; Terakura, K.; Hamada, N. Band-Structure Calculations for Boron Nitrides with Three Different Crystal Structures. *J. Phys. C* **1987**, *20*, 1241–1251.

(45) Xu, Y.-N.; Ching, W. Y. Calculation of Ground-State and Optical Properties of Boron Nitrides in the Hexagonal, Cubic, and Wurtzite Structures. *Phys. Rev. B* **1991**, *44*, 7787–7798.

(46) Goñi, A. R.; Kaess, F.; Reparaz, J. S.; Alonso, M. I.; Garriga, M.; Callsen, G.; Wagner, M. R.; Hoffmann, A.; Sitar, Z. Dependence on Pressure of the Refractive Indices of Wurtzite ZnO, GaN, and AlN. *Phys. Rev. B* **2014**, *90*, 045208.

(47) Serrano, J.; Romero, A. H.; Manjón, F. J.; Lauck, R.; Cardona, M.; Rubio, A. Pressure Dependence of the Lattice Dynamics of ZnO: An ab initio Approach. *Phys. Rev. B* **2004**, *69*, 094306.

TOC Graphic.

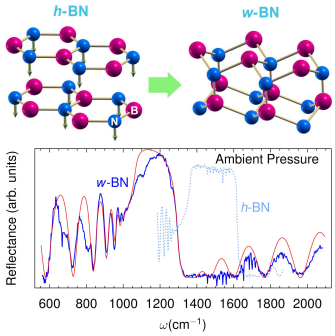
h-BN
w-BN
B
N
Ambient Pressure
w-BN
h-BN
Reflectance (arb. units)
600
800
1000
1200
1400
1600
1800
2000
ω(cm⁻¹)